Investigation into the effect of Y, Yb doping in $Ba_2In_2O_5$: determination of the solid solution range and co-doping with phosphate

J.F. Shin, P.R. Slater*

School of Chemistry, University of Birmingham, Birmingham. B15 2TT. UK

*Correspondence to

Prof. P.R. Slater
School of Chemistry
University of Birmingham
Birmingham B15 2TT
UK

p.r.slater@bham.ac.uk

Abstract

In this paper we examine the effect of Y, Yb doping in $Ba_2In_2O_5$, examining the solid solution range and effect on the conductivity and CO_2 stability. The results showed that up to 35% Y, Yb can be introduced, and this doping leads to an introduction of disorder on the oxygen sublattice, and a corresponding increase in conductivity. Further increases in Y, Yb content could be achieved through co-doping with phosphate. While this co-doping strategy led to a reduction in the conductivity, it did have a beneficial effect on the CO_2 stability, and further improvements in the CO_2 stability could be achieved through La and P co-doping.

Keywords: Perovskite, proton conductor, phosphate, indate, yttrium, ytterbium

Introduction

Oxide ion/Proton conducting ceramics have been attracting significant interest due to potential technological applications in fuel cells, separation membranes and sensors [1-3]. One system that has attracted considerable interest is $Ba_2In_2O_5$ [4-20], which adopts the brownmillerite structure, in which the oxide ion vacancies are ordered leading to alternating layers of octahedral and tetrahedral In. As a result of this vacancy ordering, the oxide ion conductivity is comparatively low, but at higher temperatures a step-wise increase in conductivity is observed due to the resultant disorder introduced during the transition from an orthorhombic to tetragonal unit cell. As a result of this observed high oxide ion conductivity in the high temperature structure of $Ba_2In_2O_5$, there have been many doping strategies investigated to stabilize the disordered structure to lower temperature. In this respect, doping with higher valent cations (e.g. Zr, Ce, Ti) with similar size have proved very effective. Such studies have also shown that the conductivity at low temperatures can be further enhanced in wet atmospheres, due to water incorporation into the oxide ion vacancies and a resultant protonic contribution to the conductivity, and particular recent interest in this respect for fuel cell applications has been in terms of Ti doped $Ba_2In_2O_5$ [21]. Our own recent studies have demonstrated that oxyanion (MO_4^{n-}; M= S, P, Si) doping is similarly successful. In such a doping strategy, the P, S, Si of the oxyanion group resides on the perovskite B cation site, with the oxide ions of this group filling 4 or the available 6 oxide ion positions around this site. In addition to enhancing the oxide ion conductivity in this and related phases through the introduction of disorder, such oxyanion doping has been shown to enhance the stability towards CO_2 (poor CO_2 stability is a key issue for applications of many potential proton

conducting electrolytes) [22-26]. However, issues with $Ba_2In_2O_5$ electrolyte materials for technological applications are the high cost of In, as well as its tendency for In^{3+} to reduce at high temperatures under reducing conditions, and so we have been investigating strategies to reduce the In content. In this respect we have examined Y, Yb doping in $Ba_2In_2O_5$. Previous studies have shown Y substitution up to 35% in $Ba_2In_2O_5$ and a similar solubility limit of Yb into the related $Ba_{0.6}Sr_{0.4}LaIn_2O_{5.5}$ [19, 20]. In this work, we expand such studies to investigate the CO_2 stability of such systems, as well as the possible incorporation of higher levels of Y, Yb through co-doping with phosphate.

Experimental

High purity $BaCO_3$, In_2O_3, La_2O_3, Y_2O_3, Yb_2O_3, and $NH_4H_2PO_4$ were used to prepare $Ba_{2-z}La_zIn_{2-x-y}M_yP_xO_{5+x+z/2}$ (M=Y, Yb) samples. A small (3%) excess of $BaCO_3$ was employed, in order to overcome Ba loss at elevated temperatures, and eliminate Ba deficient impurity phases, such as $BaIn_2O_4$, as has been seen in other studies synthesising similar Ba containing phases [22,23]. The powders were intimately ground and heated initially to 1000°C for 12 hours. They were then ball-milled (350 rpm for 1 hour, Fritsch Pulverisette 7 Planetary Mill) and reheated to 1000°C for 50 hours. The resulting powders were then ball-milled (350 rpm for 1 hour, Fritsch Pulverisette 7 Planetary Mill) a second time and pressed as pellets (1.3 cm diameter) and sintered at 1400°C for 10 hours. The pellets were covered in sample powder and the crucible was covered with a lid to limit the amount of Ba loss during the sintering process. Powder X-ray diffraction (Bruker D8 diffractometer with Cu $K\alpha_1$ radiation) was used to demonstrate phase purity

as well as for preliminary structure determination. For the latter, the GSAS suite of programs was used [27].

The CO_2 stability of samples was determined using thermogravimetric analysis (Netzsch STA 449 F1 Jupiter Thermal Analyser). Samples were heated at 10 $^{\circ}$C min^{-1} to 1000 $^{\circ}$C in 1:1 CO_2 and N_2 mixture to determine at what temperature CO_2 pick up occurred. In addition further stability studies were performed by heating samples at 600°C for 12 hours in a tube furnace under flowing CO_2 gas.

Raman spectroscopy measurements were made in order to provide further evidence for the successful incorporation of phosphate. These measurements utilised a Renishaw inVia Raman microscope with excitation using a Cobolt Samba CW 532 nm DPSS Laser.

The water contents of hydrated samples were determined from thermogravimetric analysis (Netzsch STA 449 F1 Jupiter Thermal Analyser). Samples were heated at 10°C min^{-1} to 1000°C in N_2, and the water content was determined from the observed mass loss.

For the conductivity measurements, the sintered pellets were coated with Pt paste, and then heated to 800°C for 1 hour to ensure bonding to the pellet. Conductivities were then measured by AC impedance measurements (Hewlett Packard 4192A impedance analyser) in the range from 0.1 to 10^3 kHz, with an applied voltage of 100 mV. Measurements were made in dry N_2 and wet N_2 (in which the gas was bubbled at room temperature through water) to identify any protonic contribution to the conductivity. The impedance data showed a single broad semicircle in both dry and wet atmospheres (figure 1). The capacitance of the semicircle ($\approx 10^{-12}$ F cm^{-1}) was typical of a bulk response, suggesting that the resistance of the grain boundary was small compared to that of the bulk.

Results and discussion

In the first instance, the solid solution range for Y, Yb doped $Ba_2In_2O_5$ was examined. The results showed that single phase samples of $Ba_2In_{2-y}M_yO_5$ (M=Y, Yb) could be prepared for $0 \leq y \leq 0.7$, with impurities (e.g. $Ba_3(Y/Yb)_4O_9$) being observed for higher levels of Y, Yb. The observed solid solution ranges for Y, Yb in the $Ba_2In_2O_5$ structure are similar to the range previously reported by Noirault *et al.* for Y doping in this system, and for Yb doping by Kakinuma *et al.* in the related $Ba_{0.6}Sr_{0.4}LaIn_2O_{5.5}$ [19, 20]. The results show a reduction in the orthorhombic splitting on Y, Yb incorporation, and a transition towards cubic symmetry for the highest Y, Yb levels, suggesting the introduction of disorder on the oxygen sublattice through Y, Yb doping (figure 2, table 1). The cell parameters showed an increase (comparing equivalent cells) on Y/Yb introduction, which is consistent with the larger size of Y^{3+}/Yb^{3+} compared to In^{3+}.

In agreement with the above conclusions regarding the introduction of oxygen disorder, an increase in conductivity in dry N_2 is observed on increasing Y/Yb content (figure 3, table 2), with a further increase due to a protonic contribution on changing to wet N_2, in line with prior reports [19]. The effect of Y, Yb doping on the CO_2 stability was then examined. Undoped $Ba_2In_2O_5$ shows comparatively poor CO_2 stability, with TGA studies showing a mass increase above 600°C on heating in a 1:1 CO_2 and N_2 gas mixture. The Y, Yb doped samples showed similar low stability (figure 4). In these cases the temperature at which the first mass increases was observed was slightly lower, at 550°C, for both $Ba_2In_{1.3}Y_{0.7}O_5$ and $Ba_2In_{1.3}Yb_{0.7}O_5$, although the overall mass increases were slightly lower (figure 4). In agreement with the TGA results, samples heated under CO_2 in a tube

furnace at 600°C showed the presence of significant amounts of $BaCO_3$ impurity, with the highest levels of $BaCO_3$ observed for undoped $Ba_2In_2O_5$ (figure 5).

In order to determine the level of water incorporation in these samples, they were heated under wet N_2 to 800°C, before slow cooling (0.4 °C min^{-1}) to room temperature. The water content of these samples were then determined by thermogravimetric analysis, which indicated values of 1 H_2O per formula unit, consistent with complete filling of the oxide ion vacancies.

In order to try to increase the maximum Y/Yb content, as well as improve the CO_2 stability, co-doping with phosphate was attempted. The results showed that quite high levels of phosphate were required to increase the Y/Yb content further, with it proving to be possible to prepare single phase samples with composition $Ba_2In_{0.5}(Y/Yb)P_{0.5}O_{5.5}$ (figure 6, table 3). Raman spectroscopy measurements for these phosphate doped samples are shown in figure 7. The results confirm the presence of phosphate, as exemplified by the appearance of a peak at 940 cm^{-1}. While the previous studies for Y, Yb doped $Ba_2In_2O_5$ showed a small decrease in the onset temperature of CO_2 pick-up, the addition of phosphate, despite the higher Y, Yb contents, led to a small increase in this temperature, with the $Ba_2In_{0.5}YbP_{0.5}O_{5.5}$ sample only showing a main mass increase above 700°C (figures 8 and 9). This improved CO_2 stability on phosphate doping is in agreement with prior results on phosphate doped $Ba_2In_2O_5$, which was attributed to a reduction in the basicity of the system on introducing phosphate. While the co-doping with phosphate was beneficial in terms of the CO_2 stability, the conductivity was lowered (table 4, figure 9), which is most likely due to the reduction in the oxide ion vacancy

content, and the fact that the vacancies present are essentially trapped around the phosphorus, due to its preference to incorporate as a tetrahedral PO_4^{3-} ion.

In order to try to improve the CO_2 stability further, and increase the conductivity, additional co-doping studies were performed. These experiments were directed by prior studies on $Ba_2In_2O_5$ which showed that co-doping with La and phosphate improved the CO_2 stability [25]. In agreement with these prior studies, the results here showed that co-doping $Ba_2In_{2-y}(Y/Yb)_yO_5$ with La and phosphate gave rise to a further improvement in the CO_2 stability. To accommodate the La, the phosphate content was required to be lowered, with X-ray diffraction studies showing samples of composition $Ba_{1.7}La_{0.3}In_1(Y/Yb)_{0.7}P_{0.3}O_{5.45}$ to be single phase. These samples showed good CO_2 stability, with TGA showing a mass increase on heating in a 1:1 CO_2 and N_2 gas mixture only at temperatures above 900°C (figure 8). However, while the CO_2 stability was improved, the conductivity was significantly lower than for both samples with and without phosphate (figure 10).

Conclusions

The results show that it is possible to introduce up to 35% Y, Yb into $Ba_2In_2O_5$ leading to an improvement in the low temperature conductivity as a result of the introduction of disorder on the oxygen sublattice. Further increases in Y, Yb content are possible through co-doping with phosphate. This co-doping strategy led to a small improvement in the CO_2 stability, albeit at the detriment of the conductivity. Further improvements in the CO_2 stability could be achieved through co-doping on the Ba site with La. However, the

improvement in the CO_2 stability was shown to be at the detriment of the conductivity, indicating the problems with obtaining both high conductivity and CO_2 stability.

Acknowledgements

We would like to express thanks to EPSRC (grant EP/I003932/1) and the University of Birmingham for funding (EPS international PhD scholarship for JFS). The Bruker D8 diffractometer, Renishaw inVia Raman microscope, and Netzsch STA 449 F1 Jupiter Thermal Analyser used in this research were obtained through the Science City Advanced Materials project: Creating and Characterising Next generation Advanced Materials project, with support from Advantage West Midlands (AWM) and part funded by the European Regional Development Fund (ERDF).

References

[1]. K. D. Kreuer, Annu. Rev. Mater. Res. 33 (2003) 333.

[2]. T. Norby, Solid State Ionics, 125 (1999) 1

[3]. A. Orera, P.R. Slater; Chem. Mater. 22 (2010) 675.

[4]. J.B. Goodenough, J.E. Ruizdiaz, Y.S. Zhen, Solid State Ionics 44 (1990) 21.

[5]. S.A. Speakman, J.W. Richardson, B.J. Mitchell, S.T. Misture, Solid State Ionics 149 (2002) 247.

[6]. T. Schober, Solid State Ionics 109 (1998**)** 1.

[7]. V. Jayaraman, A. Magrez, M. Caldes, O. Joubert, M. Ganne, Y. Piffard, L. Brohan, Solid State Ionics 170 (2004) 17.

[8]. A. Rolle, R.N. Vannier, N.V. Giridharan, F. Abraham, Solid State Ionics 176 (2005) 2095.

[9]. T. Schrober, J. Friedrich, Solid State Ionics 113 (1998) 369.

[10]. G.B. Zhang, D.M. Smith, Solid State Ionics 82 (1995) 153.

[11]. E. Quarez, S. Noirault, M.T. Caldes, O. Joubert, J. Power Sources 195 (2010) 1136.

[12]. M. Karlsson, A. Matic, C.S. Knee, I. Ahmed, S.G. Eriksson, L. Borjesson, Chem. Mater. 20 (2008) 3480.

[13]. F. Giannici, A. Longo, A. Balerna, K.D. Kreuer, A. Martorana, Chem. Mater. 19 (2010) 5714.

[14]. S. Noirault, S. Celerier, O. Joubert, M.T. Caldes, Y. Piffard, Solid State Ionics 178 (2007) 1353.

[15]. I. Ahmed, S.G. Eriksson, E. Ahlberg, C.S. Knee, P. Berastegui, L.G. Johansson, H. Rundlof, M. Karlsson, A. Matic, L. Borjesson, D. Engberg, Solid State Ionics 177 (2006) 1395.

[16]. K. Kakinuma, A. Tomita, H. Yamamura, T. Atake, J. Mater. Sci. 41 (2006) 6435.

[17]. C.A.J. Fisher, M.S. Islam, Solid State Ionics 118 (1999) 355.

[18]. A. Jarry, E. Quarez, K. Kravchyk, O. Joubert; Solid State Ionics 216 (2012) 11.

[19]. S. Noirault, E. Quarez, Y. Piffard, O. Joubert ; Solid State Ionics 180 (2009) 1157.

[20]. K. Kakinuma, T. Waki, H. Yamamura, T. Atake; J. Ceram Soc Jpn 117 (2009) 1364.

[21]. M. Letilly, O. Joubert and A. L. La Salle, Journal of Power Sources 206 (2012) 210.

[22]. J. F. Shin, L. Hussey, A. Orera, P. R. Slater; Chem Commun. 46 (2010) 4613.

[23]. J.F. Shin, D.C. Apperley, P.R. Slater; Chem. Mater. 22 (2010) 5945.

[24]. J.F. Shin, A. Orera, D.C. Apperley, P.R. Slater; J. Mater. Chem. 21 (2011) 874.

[25]. J.F. Shin, P.R. Slater; J. Power Sources 196 (2011) 8539.

[26]. J.F. Shin, K. Joubel, D.C. Apperley, P.R. Slater; *Dalton Trans*, 2012, **41**, 261.

[27]. A.C. Larson, R.B. Von Dreele. *Los Alamos National Laboratory, Report*. No LA-UR-86-748 (1987).

Table 1. Cell parameter data for $Ba_2In_{2-x}Y/Yb_xO_5$

Sample (nominal composition)	Unit cell parameters (Å)			Unit cell volume (Å^3)
	a	b	c	
$Ba_2In_2O_5$	6.089(2)	16.736(8)	5.963(2)	607.6(2)
$Ba_2In_{1.6}Y_{0.4}O_5$	6.025(3)	17.135(9)	6.040(2)	623.5(3)
$Ba_2In_{1.3}Y_{0.7}O_5$	4.280(1)	-	-	78.38(4)
$Ba_2In_{1.6}Yb_{0.4}O_5$	6.118(2)	16.817(9)	6.005(3)	617.8(4)
$Ba_2In_{1.3}Yb_{0.7}O_5$	4.264(1)	-	-	77.53(4)

Table 2. Conductivity data for $Ba_2In_{2-x}Y/Yb_xO_5$

Sample (nominal composition)	Conductivity (S cm^{-1})		
	500 °C		800 °C
	Wet	Dry	
$Ba_2In_2O_5$	3.2×10^{-5}	6.5×10^{-6}	1.1×10^{-3}
$Ba_2In_{1.6}Y_{0.4}O_5$	1.8×10^{-4}	4.0×10^{-5}	1.7×10^{-3}
$Ba_2In_{1.3}Y_{0.7}O_5$	2.6×10^{-3}	6.7×10^{-4}	9.5×10^{-3}
$Ba_2In_{1.6}Yb_{0.4}O_5$	1.7×10^{-4}	3.9×10^{-5}	1.4×10^{-3}
$Ba_2In_{1.3}Yb_{0.7}O_5$	4.6×10^{-4}	3.4×10^{-4}	8.1×10^{-3}

Table 3. Cell parameter data for La and/or P co-doped $Ba_2In_{2-x}Y/Yb_xO_5$

Sample (nominal composition)	Unit cell parameters (Å)			Unit cell volume ($Å^3$)
	a	b	c	
$Ba_2In_2O_5$	6.089(2)	16.736(8)	5.963(2)	607.6(2)
$Ba_2In_{0.5}Y_1P_{0.5}O_{5.5}$	4.269(1)	-	-	77.78(4)
$Ba_2In_{0.5}Yb_1P_{0.5}O_{5.5}$	4.244(1)	-	-	76.43(4)
$Ba_{1.7}La_{0.3}In_1Y_{0.7}P_{0.3}O_{5.45}$	4.241(1)	-	-	76.25(4)
$Ba_{1.7}La_{0.3}In_1Yb_{0.7}P_{0.3}O_{5.45}$	4.221(1)	-	-	75.23(4)

Table 4. Conductivity data for La and/or P co-doped $Ba_2In_{2-x}Y/Yb_xO_5$

Sample (nominal composition)	Conductivity (S cm^{-1})		
	500 °C		800 °C
	Wet	Dry	
$Ba_2In_2O_5$	3.2×10^{-5}	6.5×10^{-6}	1.1×10^{-3}
$Ba_2In_{0.5}Y_1P_{0.5}O_{5.5}$	4.5×10^{-4}	1.7×10^{-4}	4.4×10^{-4}
$Ba_2In_{0.5}Yb_1P_{0.5}O_{5.5}$	6.6×10^{-4}	2.0×10^{-4}	6.1×10^{-4}
$Ba_{1.7}La_{0.3}In_1Y_{0.7}P_{0.3}O_{5.45}$	3.3×10^{-4}	9.8×10^{-5}	1.5×10^{-3}
$Ba_{1.7}La_{0.3}In_1Yb_{0.7}P_{0.3}O_{5.45}$	2.7×10^{-4}	8.3×10^{-5}	1.3×10^{-3}

Figure Captions

Fig. 1. Impedance spectra for $Ba_2In_{1.3}Yb_{0.7}O_5$ at 260 °C: dry N_2 (square) and wet N_2 (cross).

Fig. 2. XRD patterns for (a) $Ba_2In_2O_5$, (b) $Ba_2In_{1.6}Y_{0.4}O_5$, (c) $Ba_2In_{1.3}Y_{0.7}O_5$, (d) $Ba_2In_{1.6}Yb_{0.4}O_5$ and (e) $Ba_2In_{1.3}Yb_{0.7}O_5$.

Fig. 3. Conductivity data in dry N_2 for $Ba_2In_2O_5$ (open circle), $Ba_2In_{1.6}Y_{0.4}O_5$ (open triangle), $Ba_2In_{1.3}Y_{0.7}O_5$ (open diamond), $Ba_2In_{1.6}Yb_{0.4}O_5$ (open square), $Ba_2In_{1.3}Yb_{0.7}O_5$ (open cross). Conductivity data in wet N_2 for $Ba_2In_{1.3}Y_{0.7}O_5$ (filled diamond) is also shown.

Fig. 4. TG profiles (10 °C min^{-1} to 1000 °C in 1:1 CO_2 and N_2 mixture) for $Ba_2In_2O_5$ (circle), $Ba_2In_{1.3}Y_{0.7}O_5$ (triangle) and $Ba_2In_{1.3}Yb_{0.7}O_5$ (square).

Fig. 5. XRD patterns for (a) $Ba_2In_2O_5$, (b) $Ba_2In_{1.3}Y_{0.7}O_5$ and(c) $Ba_2In_{1.3}Yb_{0.7}O_5$ after heating in CO_2 at 600 °C for 12h.

Fig. 6. XRD patterns for (a) $Ba_2In_{0.5}Y_1P_{0.5}O_{5.5}$, (b) $Ba_2In_{0.5}Yb_1P_{0.5}O_{5.5}$, (c) $Ba_{1.7}La_{0.3}In_1Y_{0.7}P_{0.3}O_{5.45}$ and (d) $Ba_{1.7}La_{0.3}In_1Yb_{0.7}P_{0.3}O_{5.45}$.

Fig. 7. Raman spectra of (a) $Ba_2Yb_{1.5}P_{0.5}O_{5.5}$ (b) $Ba_2In_{0.5}Yb_1P_{0.5}O_{5.5}$ (c) $Ba_{1.7}La_{0.3}In_1Yb_{0.7}P_{0.3}O_{5.45}$ and (d) $Ba_3(PO_4)_2$

Fig. 8. TG profiles (10 °C min^{-1} to 1000 °C in 1:1 CO_2 and N_2 mixture) for $Ba_2In_{0.5}Y_1P_{0.5}O_{5.5}$ (open triangle), $Ba_2In_{0.5}Yb_1P_{0.5}O_{5.5}$ (open square), $Ba_{1.7}La_{0.3}In_1Y_{0.7}P_{0.3}O_{5.45}$ (closed triangle) and $Ba_{1.7}La_{0.3}In_1Yb_{0.7}P_{0.3}O_{5.45}$ (closed square).

Fig. 9. XRD patterns for (a) $Ba_2In_{0.5}Y_1P_{0.5}O_{5.5}$, (b) $Ba_2In_{0.5}Yb_1P_{0.5}O_{5.5}$ (c) $Ba_{1.7}La_{0.3}In_1Y_{0.7}P_{0.3}O_{5.45}$ and (d) $Ba_{1.7}La_{0.3}In_1Yb_{0.7}P_{0.3}O_{5.45}$ after heating in CO_2 at 600 °C

for 12h, showing no evidence for $BaCO_3$ formation unlike for samples without P doping (see figure 4).

Fig. 10. Conductivity data in dry N_2 for $Ba_2In_{0.5}Y_1P_{0.5}O_{5.5}$ (open square), $Ba_2In_{0.5}Yb_1P_{0.5}O_{5.5}$ (open diamond), $Ba_{1.7}La_{0.3}In_1Y_{0.7}P_{0.3}O_{5.45}$ (open triangle) and $Ba_{1.7}La_{0.3}In_1Yb_{0.7}P_{0.3}O_{5.45}$ (open circle). Conductivity data in wet N_2 for $Ba_2In_{0.5}Y_1P_{0.5}O_{5.5}$ (filled square) and $Ba_{1.7}La_{0.3}In_1Y_{0.7}P_{0.3}O_{5.45}$ (filled triangle) are also shown.

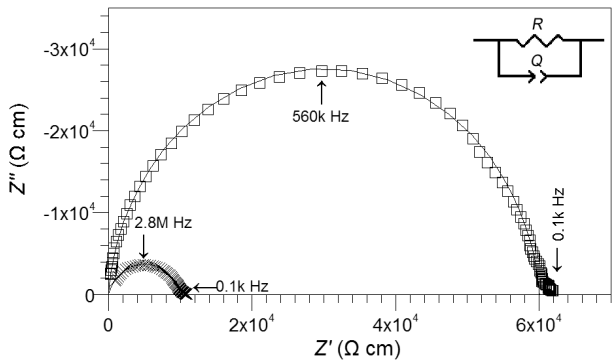
R
Q
-3x10^4
-2x10^4
-1x10^4
0
Z'' (Ω cm)
560k Hz
2.8M Hz
0.1k Hz
0.1k Hz
0
2x10^4
4x10^4
6x10^4
Z' (Ω cm)

Fig. 1

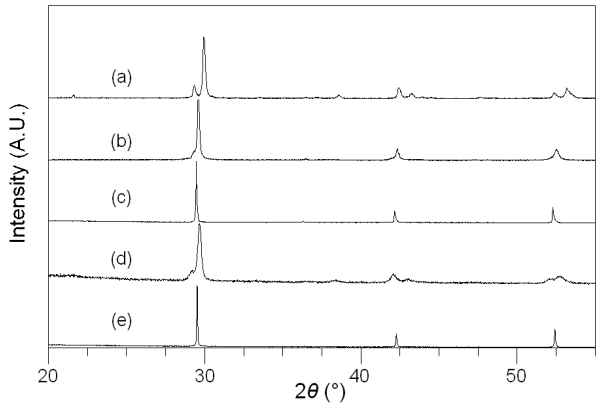

Fig 2.

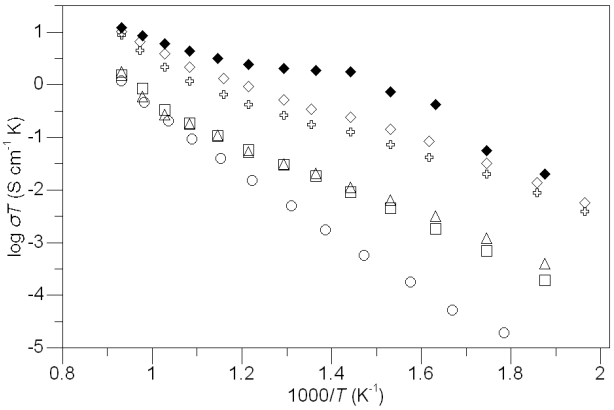

Fig. 3

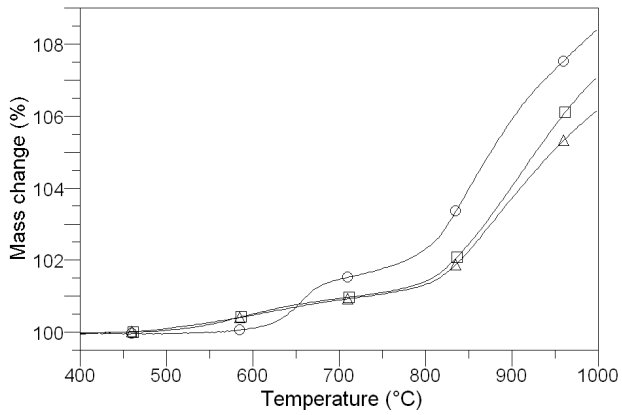
Mass change (%)
108
106
104
102
100
400
500
600
700
800
900
1000
Temperature (°C)

Fig. 4

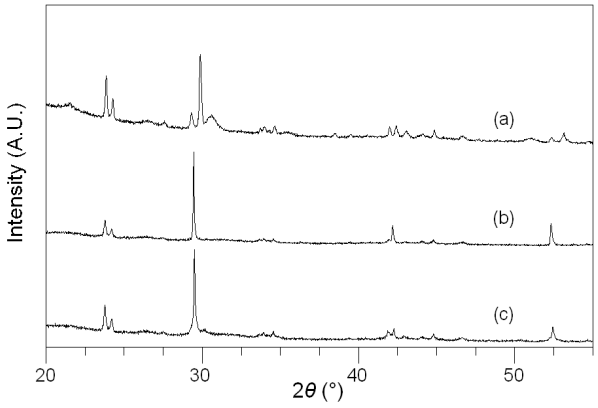

Fig. 5

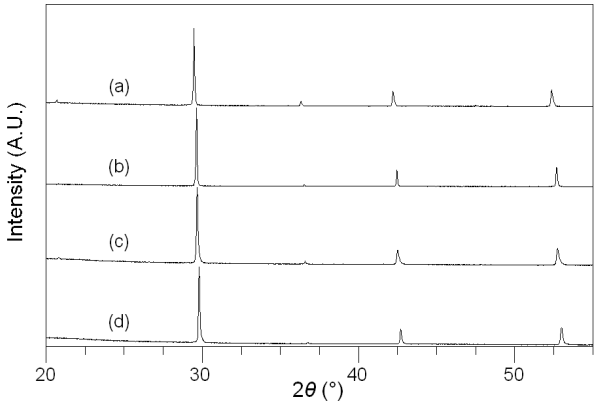

Fig. 6

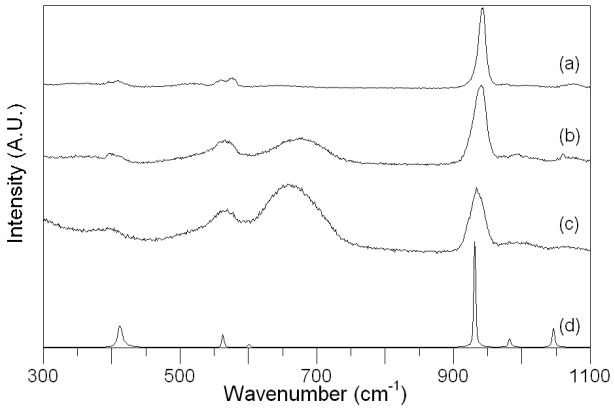

Fig. 7.

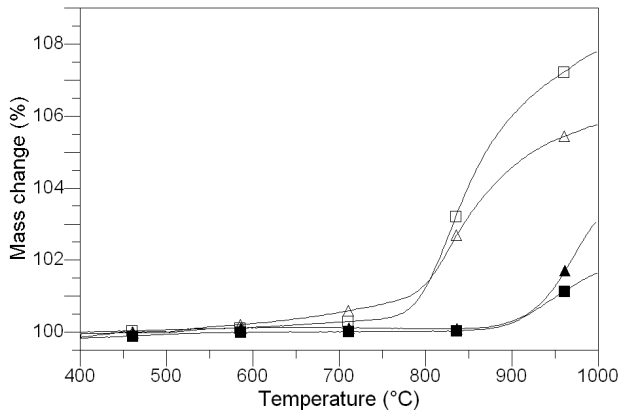
Mass change (%)
108
106
104
102
100
400
500
600
700
800
900
1000
Temperature (°C)

Fig. 8.

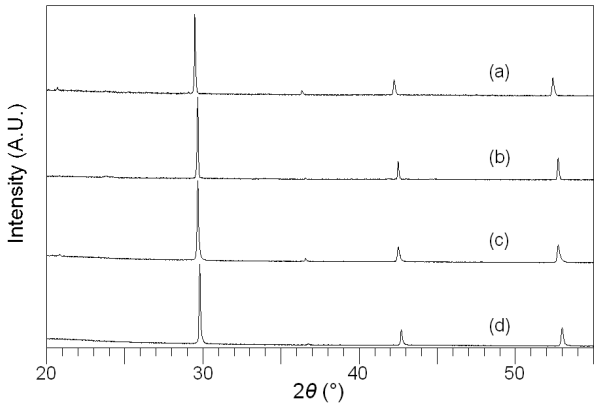

Fig 9.

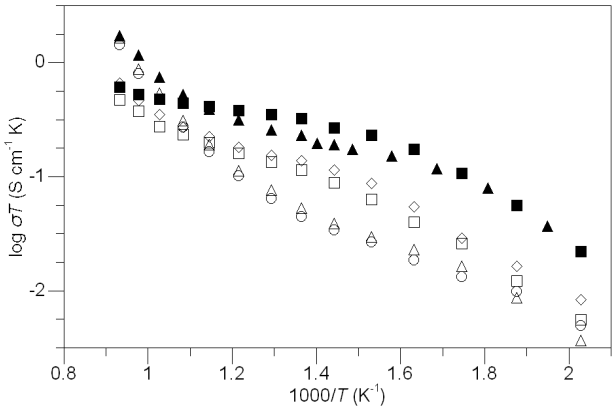

Fig. 10